Published in final edited form as:
*Cell Metab*. 2019 June 10; 30(3): 594–606.e3. doi:10.1016/j.cmet.2019.06.002.

# Systems-level quantitative analysis of inter-organ metabolite exchange in pigs

**Cholsoon Jang**[1], **Sheng Hui**[#1], **Xianfeng Zeng**[#1], **Alexis J. Cowan**[1], **Lin Wang**[1], **Li Chen**[1], **Raphael J. Morscher**[1], **Jorge Reyes**[1], **Christian Frezza**[2], **Ho Young Hwang**[3], **Akito Imai**[3], **Yoshiaki Saito**[3], **Keitaro Okamoto**[3], **Christine Vaspoli**[3], **Loewe Kasprenski**[3], **Gerald A. Zsido II**[3], **Joseph H. Gorman III**[3], **Robert C. Gorman**[3], **Joshua D. Rabinowitz**[1,*]

[1]Department of Chemistry and Lewis-Sigler Institute for Integrative Genomics, Princeton University, Princeton, NJ USA 08544

[2]Medical Research Council Cancer Unit, Hutchison/MRC Research Centre, University of Cambridge, Cambridge, UK

[3]Perelman School of Medicine, University of Pennsylvania, 3400 Civic Blvd, Philadelphia, PA USA 19104

[#] These authors contributed equally to this work.

## Summary

Mammalian organs continually exchange metabolites via circulation, but systems-level analysis of this shuttling process is lacking. Here we compared, in fasted pigs, metabolite concentrations in arterial blood versus draining venous blood from 11 organs. Greater than 90% of metabolites showed arterial-venous differences across at least one organ. Surprisingly, the liver and kidneys released not only glucose but also amino acids, both of which were consumed primarily by the intestine and pancreas. The liver and kidneys exhibited additional unexpected activities: liver preferentially burned unsaturated over more atherogenic saturated fatty acids, while the kidneys were unique in burning circulating citrate and net oxidizing lactate to pyruvate, thereby contributing to circulating redox homeostasis. Furthermore, we observed more than 700 other cases of tissue-specific metabolite production or consumption, such as release of nucleotides by the spleen and TCA intermediates by pancreas. These data constitute a high-value resource, providing quantitative atlas of inter-organ metabolite exchange.

[*]The Lead Contact: joshr@princeton.edu (J.D.R.).

**Author Contributions**

C.J., R.J.M., and J.D.R. designed the study. C.J. performed the most experiments. S.H., contributed to isotope tracing studies in pigs and mice, modeling, and data analysis. X.Z. contributed to isotope tracing studies in mice, developed the analytical method for SCFA, and collected the SCFA data. A.J.C. contributed to pig experiments and sample preparation. J.R. contributed to the flux analysis. L.W. and L.C. contributed to chemical formula assignment of putative metabolites. C.F. contributed the ideas on kidney cancer. H.Y.H., A.I., Y.S., K.O., C.V., L.K., and G.A.Z. performed pig surgery and blood collection. J.H.G. and R.C.G. provided surgical expertise and intellectual guidance. C.J., and J.D.R. wrote the manuscript. All authors discussed the results and commented on the manuscript.

**Declaration of Interests**

Authors declare no competing interests.


Europe PMC Funders Author Manuscripts

## Introduction

Converting environmental nutrient inputs, whose availability is often unreliable, into energy and biomass is a fundamental challenge of life. Unicellular organisms, like bacteria or yeasts, face this challenge in each cell individually. An important advantage of multi-cellularity is the ability of cells to work in concert to achieve metabolic homeostasis (Chantranupong et al., 2015). This in turn allows organs to develop specialized metabolism, which is adapted to their particular biological function, with metabolites produced in one organ transmitted to another organ via the circulatory system.

The biological significance of metabolite exchange has been recognized since the discovery of the Cori cycle (Cori, 1981), in which lactate made by skeletal muscle is converted into glucose by the liver. Since then, other examples of metabolite exchange have been elucidated (e.g., alanine cycle between the liver and muscle, glutamate-glutamine cycle between neurons and astrocytes) (Felig, 1973; Bak et al., 2006). However, these findings are limited to only a few metabolites and organs. Comprehensive mapping of inter-organ metabolite exchange has not yet been achieved. Understanding the production and consumption sites of circulating metabolites is important, because it can facilitate diagnosis or treatment of diseases involving either the organ or metabolite. In addition, it is key to understanding the integrative function of mammalian metabolism.

Each organ is fed by arterial blood and drained by venous blood (with the liver also fed by the portal vein from the intestine). Measurement of arterio-venous (AV) concentration differences is a well-established approach for quantification of organ-specific metabolite production and consumption (Cantarow and Ricchiuti, 1934; Hickam et al., 1948; Ivanisevic et al., 2015). To investigate metabolite exchange between organs, we performed metabolomics in the arterial blood, the organ-specific draining veins, and the urine of pigs. We chose pigs because their diet and metabolism are remarkably similar to humans (Perleberg et al., 2018; Prather et al., 2008). In addition, their large size ensures adequate blood volume and results in 11 different draining veins being sufficiently large to sample reliably. These include veins draining many major metabolic organs (liver, kidney, intestine, colon, spleen, pancreas, heart, lung, brain). Ear vein was selected because it is enriched in draining from skin. No accessible vein selectively drains from adipose, with the femoral vein draining both adipose and major leg muscles.

To confirm the generality of key observations from the pig AV concentration difference measurements, we utilized *in vivo* isotope tracing in mice. In this manner, we verified several key insights from the pig AV data, such as use of citrate to fuel the kidney and preferential hepatic catabolism of unsaturated over saturated fatty acids. This holistic analysis of metabolite exchange revealed sources and sinks of the circulating metabolome, resulting in a fundamental dataset containing over 700 significant cases of organ-specific metabolite production or consumption. Collectively, this resource illuminates the metabolic roles of mammalian organs.

Europe PMC Funders Author Manuscripts

## Results and Discussion

### General features of metabolite exchange

To obtain arterial and venous blood for measuring metabolite exchange, overnight-fasted adult pigs (~50 kg) were briefly anesthetized and blood was drawn from the arterial circulation and organ-specific draining veins (Fig. 1A). For each vascular bed, we calculated the $\log_2$ ratio of metabolite abundance in the draining vein ($C_v$) relative to the systemic arterial blood ($C_a$) (Fig. 1B). Values of $\log_2$ ($C_v/C_a$) greater than zero indicate net release, whereas values less than zero indicate net uptake. Because the liver is fed both by the hepatic artery (22%) and the portal vein (78%) (Eipel et al., 2010), we used a weighted average of these two inputs to determine metabolite concentrations feeding the liver. Multiple organs drain into the hepatic portal vein (e.g., spleen, pancreas, and intestines), which we collectively refer to as the other visceral organs (Fig. 1C).

A challenge with measuring metabolite exchange based on AV concentration differences is that, due to the speed of vascular flow, biologically important uptake and excretion fluxes may cause only small AV differences, especially for abundant metabolites. Accordingly, precise measurements are required. To enhance measurement precision, blood was drawn from each vessel twice, and each resulting serum sample was independently extracted and measured by LC-MS three times. Figures show the median value of each independent blood draw. Statistical analyses were conducted using a single value for each pig (the average of the two independent blood draws), with N = the number of pigs (Fig. 1D).

Our metabolomics methods measure ~ 600 known small molecule metabolites, whose identities were confirmed by exact mass and retention time match to authenticated standards. Among these, 280 metabolites were detected in the pig serum (Fig. 1E), with 91% showing statistically significant AV differences for at least one organ (Fig. 1E and 1F). In total, we detected 739 statistically significant cases of organ-specific metabolite production or consumption (Table 1 and Data File 1). These were roughly equally distributed across abundant and less abundant metabolites (Fig. S1).

Heat map analysis revealed a few overarching trends (Fig. 1G and Data Files 2 and 3). Consistent with their key role in waste removal, the kidneys clear ~ 50% of circulating metabolites, some of which are made by nearly every other organ (note the long blue column in the heat map). Many other metabolites are cleared by the liver (top and bottom on heat map), with the strongest changes occurring in microbiome-derived products made in the intestine (top of heat map). Conversely, the liver also releases many metabolites, including many amino acids, which are consumed by the rest of the body, especially the other visceral organs (middle of heat map).

In addition to these general patterns, certain metabolites have specific production and consumption sites (distinctive thin yellow or blue lines in the heat map). Table 2 summarizes the three most substantially produced and consumed metabolites for each organ, taking into account both the statistical significance and AV fold-change. Table S1 summarizes sinks and sources of each metabolite.

Untargeted metabolomics also identified many unannotated ions with significant AV differences. Among them, we assigned chemical formulas to 55 putative metabolites (after exclusion of adducts and isotopic variants), based on accurate mass, natural isotopic distribution and MS/MS (Fig. S2). Examples include $C_{20}H_{34}O_9$, produced only by the leg, and $C_7H_7NO_4$, produced by the liver. The existence of these organ-specific production and consumption patterns provides a particular motivation to identify these compounds.

## Kidney metabolism

The primary role of the kidneys is waste excretion. This is achieved by filtration of the blood and reabsorption of salt and circulating nutrients. Kidneys also produce glucose and other specific metabolites, including glycocyamine (creatine precursor) and serine (Fig. 2A). Patients with the kidney failure display significantly lower circulating levels of glycocyamine (Kikuchi et al., 1981). We also identified guanosine, allantoate, and phenylacetate as additional kidney-specific metabolic products, which may be useful diagnostic markers for renal dysfunction.

Among the much larger set of metabolites that are cleared by the kidneys, we observed a strong correlation between the metabolite's absolute concentration in the blood, and its reabsorption efficiency, with more abundant metabolites being more effectively reabsorbed (Fig. 2B). Notable exceptions to this trend were classical metabolic waste products such as uric acid and creatinine. For this analysis, we omitted fatty acids and acylcarnitines, which are relatively hydrophobic and were retained in blood regardless of their concentrations (Fig. S3A), perhaps because they are bound to circulating albumin and thus never filtered. The correlation between reabsorption efficiency and plasma concentration of water-soluble metabolites is consistent with an evolutionary drive to avoid wasting of abundant circulating metabolites. It also suggests that renal reabsorption efficiency is a major determinant of circulating metabolite levels.

The kidneys' continuous reabsorption against metabolite concentration gradients demands substantial energy. What feeds the kidneys? Strikingly, kidneys were distinguished by taking up circulating TCA intermediates, the most abundant of which is citrate (Fig. 2C). Indeed, citrate showed the fourth largest renal uptake after lactate, uric acid, and glutamine (Fig. S3B). To determine the fate of these species, we intravenously infused a tracer amount of $^{13}$C-labeled citrate, malate, or succinate into mice. Measurement of tissue TCA intermediates revealed a large contribution of citrate to the kidney TCA cycle (Fig. 2D). This is an intrinsic aspect of renal metabolism, as the infusion was non-perturbative (10% circulating citrate labeling, no detectable change in circulating citrate concentration; Fig. S3C). Malate and succinate did not make a comparable contribution in kidney, nor did any of these make a major contribution in other organs (Fig. S3D). The quantitative contribution of circulating citrate to the kidney TCA cycle was 20%, in the same range as glutamine and lactate (Hui et al., 2017). Thus, the kidneys are exceptional in using circulating citrate as fuel.

The ability of the kidney to catabolized citrate has been known for some time (Baruch et al., 1975; Hamm, 1990; Simpson, 1967), although the quantitative extent and uniqueness of this metabolic function had not been previously determined. The innate capacity of the kidneys

to catabolize citrate may explain key features of kidney cancer, whose rate is steadily increasing (Chow et al., 1999). Mutations in enzymes of the left side of the TCA cycle (succinate dehydrogenase and fumarate hydratase) are oncogenic (Sullivan et al., 2013). These mutations cause cancer through epigenetic mechanisms that are not kidney-specific—inhibition of α-ketoglutarate-dependent demethylases—but the mutations nevertheless occur primarily in cancers of the kidneys (Raimundo et al., 2011). This may reflect the mutations being detrimental in other tissues, as they block endogenous citrate synthesis, but not in the kidneys which can consume citrate from the circulation. While TCA mutations are relatively rare, citrate usage may more generally impact the properties of renal cancer. Clear cell renal cell carcinoma is exceptionally lipid-laden, and shows overexpression of ATP citrate lyase, which converts citrate into lipid precursors (Teng et al., 2018). Thus, high citrate uptake may shape both the mutational landscape and pathophysiology of kidney cancer (Ricketts et al., 2018).

## Exchange of glucose and lactate

To maintain circulating metabolite homeostasis, for each metabolite, total production and consumption across all organs must balance (accounting for net uptake from the diet and net excretion to urine and feces) (Fig. 3A). For an organ *i*, the net flux ($F_i$) can be calculated from the AV difference data and literature data for absolute metabolite concentrations and regional blood flow:

$$Fi = Q_i * C_a * (R_i - 1) \quad \text{(Equation 1)}$$

where $Q_i$ is the organ's blood flow, $C_a$ is the absolute metabolite concentration in the arterial blood, and $R_i$ is the measured relative concentration ratio between the draining vein of organ *i* and the arterial blood. Whole body production or consumption fluxes can then be calculated as

$$F_{production\ total} = \Sigma\ F_i\ for\ all\ F_i > 0 \quad \text{(Equation 2)}$$

$$F_{consumption\ total} = \Sigma\ F_i\ for\ all\ F_i < 0 \quad \text{(Equation 3)}$$

To maintain circulating concentration homeostasis, production and consumption fluxes must be balanced. Hence, at steady-state

$$\Sigma\ F_i = 0 \quad \text{(Equation 4)}$$

Note that this approach requires measurement of absolute metabolite AV concentration gradients, not just relative changes. Absolute concentration differences were obtained by multiplying AV fold-changes by known absolute mammalian metabolite concentrations.

Using this approach, we find that, consistent with prior literature (Stumvoll et al., 1998), the liver and kidneys produce ~68% and ~32% of circulating glucose (Fig. 3B and 3C). Strikingly, in the studied context of fasted anesthetized pig, this glucose is consumed largely by the other visceral organs (~60%) (Fig. 3B and 3C). Overall, glucose production and consumption were well-balanced, supporting this quantitative flux interpretation of AV difference data (Fig. 3C).

Lactate is a major secreted product of glucose catabolism, and also a major fuel for gluconeogenesis (Stumvoll et al., 1998). Consistent with this, lactate showed the opposite exchange patterns to glucose (Fig. 3B and 3D). Lactate and pyruvate share the same carbon skeleton, differing only in redox state. Pyruvate exhibited a similar pattern of organ-specific production and consumption to lactate, with one notable exception: The kidneys that take up lactate but release pyruvate (Fig. S4A and S4B). Thus, the kidneys net oxidize lactate to pyruvate, and thereby contribute to circulating redox homeostasis. Consistent with this notion, the chronic kidney disorders are associated with systemic redox imbalance (Poulianiti et al., 2016).

Interestingly, although glucose is the most abundant circulating carbohydrate, isotope tracer studies have shown that lactate has higher total flux into and out of the circulation. This observation is based on $^{13}$C- or $^{14}$C-isotope tracer studies, dating back decades, which measure the whole body rate of a metabolite's release from organs into the blood (endogenous production rate) (Coggan, 1999). As endogenous production rate must balance at steady-state with the rate of organ consumption and metabolic transformation, we term these rates the metabolite's circulatory turnover flux ($F_{circ}$) (Hui et al., 2017). The high $F_{circ}$ of lactate aligns with recent evidence from $^{13}$C-tracing that circulating lactate is a major TCA substrate, with glucose feeding the TCA cycle largely via circulating lactate (Hui et al., 2017; Faubert et al., 2017). Note that $^{13}$C-lactate tracing monitors the total of flux of lactate from the bloodstream into tissues and its subsequent carbon transformation (i.e. conversion to pyruvate and subsequent conversion of pyruvate to acetyl-CoA or oxaloacetate). Mere exchange of circulating lactate for tissue pyruvate does not alter the carbon skeleton of lactate and therefore does not contribute to $F_{circ}$ measured with $^{13}$C-lactate infusion. We confirmed the higher $F_{circ}$ of lactate than glucose by $^{13}$C-glucose and $^{13}$C-lactate infusion in fasted anesthetized pigs (Fig. 3F).

Compared to lactate, however, glucose shows substantially greater exchange across organs ($F_{total}$) (Fig. 3F). How can these observations be reconciled? Apparently, many organs both produce and consume circulating lactate (i.e. convert circulating glucose to circulating lactate, while also taking in circulating lactate and catabolizing it via the TCA cycle). This reflects the ubiquitous expression of monocarboxylate transporters, which render lactate a nearly universal carbohydrate fuel. Because of the simultaneous lactate consumption and production within an organ (likely by different cells of the organ), lactate exchange between organs is much less than its circulatory turnover flux. In contrast, glucose production and consumption are largely segregated across organs, with the liver and kidneys gluconeogenic and most other organs not producing circulating glucose (Stumvoll et al., 1998). This is evident in the glucose excretion by the liver and kidneys matching closely the whole body endogenous production rate ($F_{circ}$) as measured by isotope tracing (Fig. 3F). Thus, at least in

fasted pigs, only the liver and kidneys release substantial glucose into the bloodstream, whereas many organs contain cells that convert glucose to circulating lactate and also cells that take in and metabolize lactate.

## Exchange of amino acids

The amino acid with the highest plasma concentration is glutamine, which is an important energy source, gluconeogenic substrate, and nitrogen carrier (Smith, 1990). Consistent with previous AV data in human arm (Ivanisevic et al., 2015), we observed extensive glutamine production by the leg, presumably mainly from skeletal muscle (Fig. 4A). The leg's release of glutamine is in part supported by uptake of glutamate. Glutamine release, however, exceeds glutamate consumption by almost an order of magnitude. Thus, the extremities net release not only nitrogen, but also the shared glutamine/glutamate carbon skeleton (Figs. 4A and S5A). The liver, conversely, consumes glutamine and excretes glutamate (Fig. 4A), presumably passing the nitrogen from glutamine into the urea cycle (Smith, 1990). Notably, liver excretion of glutamate slightly exceeds consumption of glutamine, arguing against their shared carbon skeleton being a major net driver of hepatic gluconeogenesis (Stumvoll et al., 1998). In contrast, the other visceral organs and kidneys consume both glutamine and glutamate (Fig. 4A), raising the possibility that the glutamine carbon skeleton is an important precursor for renal glucose production.

Serine and glycine, which interconvert via folate metabolism, are another pair of high flux non-essential amino acids (Ducker and Rabinowitz, 2017). Serine and glycine were produced mainly by the kidneys (Fig. 4B), arguing for an important role of renal metabolism in systemic one-carbon homeostasis (Gottlieb and Vousden, 2017).

Essential amino acids (EAAs) cannot be synthesized by mammals and accordingly, in the fasted state, are only produced from protein breakdown. Skeletal muscle is generally believed to be the major amino acid storage organ (Lundholm et al., 1987). In contrast to this paradigm, we observed net uptake of essential amino acids by the leg, with circulating essential amino acid levels maintained by release from the liver and, surprisingly, also the kidneys (Fig. 4C). These findings are consistent with recent data that the liver expands during feeding and contracts during fasting (Sinturel et al., 2017), and suggest that the kidneys may also store protein during feeding and release it during fasting.

Where are these amino acids going? The greatest uptake of both essential and non-essential amino acids occurred in the other visceral organs (Figs. 4A-4C and S5B). To examine whether these amino acids were being used for protein synthesis, we carried out $^{13}$C-leucine tracer infusion in mice to achieve steady-state labeling of leucine (~15%) in systemic blood (Fig. S5C). The liver and kidneys, which showed net release of leucine in pigs (Fig. S5B), also incorporated $^{13}$C-leucine into proteins (Fig. 4D), suggesting that these organs simultaneously synthesize and degrade protein. But we observed the fastest protein production in the other visceral organs, which were the greatest amino acid consumers (Fig. 4D). Thus, perhaps to support continuous epithelial barrier maintenance and excretory enzyme synthesis, the pancreas and small intestine are persistently anabolic and major resting nutrient consumers.

Europe PMC Funders Author Manuscripts

Collectively, these data contrast with the common assumption that skeletal muscle is the major amino acid depot, releasing amino acids during fasting to supply energy and gluconeogenic precursors to liver and other organs. Instead, we find that the leg consumes essential amino acids, while liver and kidneys produce them. Thus, the present data argues for revisiting the basics of fasting amino acid homeostasis.

### Exchange of short- and long-chain fatty acids

In addition to being the greatest consumer of glucose and amino acids, the intestines produce a unique set of metabolites from gut microbiota (Fig. 1G). The most abundant ones are short-chain fatty acids (SCFAs) (Wu et al., 2016). Propionate and butyrate are high in the portal and colonic veins but low in the hepatic vein, confirming their synthesis by microbiota in the gut and efficient clearance by the liver (Fig. S6A) (Chambers et al., 2018). The most abundant SCFA is acetate. In addition to acetate being released by the gut, acetate is also substantially released from the head (Fig. 5A), suggesting that the brain may synthesize acetate. The acetate is then consumed by several organs including the liver, spleen, legs, and kidneys (Fig. 5A). To explore the fate of acetate in these organs, we conducted steady-state $^{13}$C-acetate tracer infusions in mice (~20% circulating labeling) (Fig. S6B). The data revealed that these consuming organs use acetate as fuel for TCA metabolism and as substrates for ketone body and fatty acid synthesis (Fig. S6C).

In contrast to the SCFAs, non-esterified long-chain fatty acids (LCFAs) are released by most organs, with the notable exceptions of the liver and heart (Fig. 5B). We suggest that this release is mainly from adipose stores, which are spread throughout the body (Björntorp, 1991). Additionally, hydrolysis of circulating triglycerides by lipoprotein lipase may contribute (Barrows et al., 2005). Liver is well known to consume LCFAs, both as an energy source and for packaging into lipoproteins (Barrows et al., 2005). Detailed analysis of LCFA species, however, revealed an unexpected preference for the liver to consume unsaturated (as opposed to saturated) LCFAs (Fig. 5C). Correspondingly, the leg preferentially takes up saturated LCFAs whereas it releases certain unsaturated ones (Fig. 5D). We also calculated the absolute exchange fluxes of the three most abundant circulating LCFAs (C16:0, C18:1 and C18:2). The analysis indicated that C18:1 and C18:2 are the high flux carbon shuttles, being released from the legs and consumed mainly in the liver (Fig. 5E). Using $^{13}$C-LCFA isotope tracing in mice, we confirmed preferential hepatic oxidation of unsaturated versus saturated LCFAs (Fig. 5F), which is consistent with preferential hepatic uptake of unsaturated LCFAs in pigs (Fig. 5E). Thus, the existence of double bond(s) in LCFAs plays critical roles in determining uptake and oxidation efficacies by organs, which may be linked to differential effects of saturated versus unsaturated LCFAs on cardiovascular and metabolic disease (Jha et al., 2018).

## Conclusions and Future Perspectives

Here we provide a quantitative atlas of inter-organ metabolite exchange. In addition to confirming classical organ-specific metabolic functions like renal and hepatic glucose production, our systems-level analysis identified unexpected ones. These include previously unknown sources and sinks for hundreds of metabolites, with 739 total observations of

significant organ-specific metabolite production or consumption (Table S1 and Data File 1). Many of these observations involve less studied metabolites, and provide a foundational resource for understanding their physiological role and homeostatic mechanisms. Even for glucose itself, we obtained new insights, most notably extensive glucose consumption by the visceral organs, highlighting an underappreciated role of the intestine, which can be gluconeogenic in some contexts (Mithieux, 2005; Jang et al., 2018), in clearing fasting blood glucose.

Looking forward, a key challenge is quantitative integration of AV difference and isotope tracing data. These two data types are complementary, as AV difference data measure *net* metabolic activity (production minus consumption) whereas isotope tracing measures *gross* metabolic activity (total production or consumption). When these align, conceptual understanding is straightforward, e.g. we find that the liver preferentially consumes and burns unsaturated versus saturated fatty acids. Differences, however, can also be highly informative. For example, although we observe a propensity for net fatty acid release from the leg, isotope tracing showed that fatty acids are a major muscle fuel (Guo and Jensen, 1998). This reflects the physiology of the body part, with adipose and muscle in proximity and playing different metabolic roles in fat management.

In sum, our data provide a comprehensive resource of net organ-specific production and consumption fluxes. These are critical inputs for ongoing efforts to quantitatively model mammalian metabolism (Ahn et al., 2017; Noronha et al., 2017; Thiele et al., 2013; Shlomi et al., 2008). As such, they are a key step towards understanding the homeostasis of the circulating metabolome.

## Limitations of Study

The AV difference measurements reported here are based on fasted, anesthetized pigs. They reflect the integrative function of the cell types and organs drained by the sampled vein (for example, internal jugular vein drains not only the brain, but also the face). Metabolism can change dramatically between feeding and fasting. Some anticipated metabolic changes in the fed state include absorption of copious glucose and amino acids from the intestinal lumen, altered access of the microbiome to dietary nutrients (Gentile and Weir, 2018), and insulin-induced muscle glucose catabolism and suppression of adipose lipolysis (Saltiel, 2015). The present measurements may also have been impacted by anesthesia, which alters brain glucose usage (Bascuñana et al., 2019) and may also impact skeletal muscle metabolism due to deficient afferent CNS inputs and associated lack of muscle contraction. Anesthesia facilitated blood sampling, especially from deeply buried veins like the hepatic, splenic and colonic. It is not, however, required for sampling from more accessible sites, and AV studies have previously been conducted in awake humans and dogs (Davis et al., 1985; Felig and Wahren, 1971; Felig et al., 1969; Moore et al., 1998; Wahren et al., 1972). Studies sampling from a more limited set of veins in awake mammals are a valuable complement to the present research, and can potentially be coupled to physiological manipulations of metabolic demand (e.g., exercise, thinking). Comprehensive AV measurements in fed animals are a key future objective.

# Star Methods

### Key Resources Table

| REAGENT or RESOURCE | SOURCE | IDENTIFIER |
|---|---|---|
| **Chemicals, Peptides, and Recombinant Proteins** | | |
| L-LACTATE (U-13C, 98%) | Cambridge Isotope Laboratories | Cat#CLM-1579-PK |
| D-GLUCOSE (U-13C, 99%) | Cambridge Isotope Laboratories | Cat#CLM-1396-PK |
| CITRATE (U-13C, 98%) | Cambridge Isotope Laboratories | Cat#CLM-9021-PK |
| L-MALATE (U-13C, 99%) | Cambridge Isotope Laboratories | Cat#CLM-8065-PK |
| SUCCINATE (U-13C, 99%) | Sigma | Cat#491985 |
| ACETATE (U-13C, 99%) | Cambridge Isotope Laboratories | Cat#CLM-440-PK |
| OLEATE (U-13C, 98%) | Cambridge Isotope Laboratories | Cat#CLM-8763-PK |
| LINOLEATE (U-13C, 98%) | Cambridge Isotope Laboratories | Cat#CLM-8735-PK |
| PALMITATE (U-13C, 98%) | Cambridge Isotope Laboratories | Cat#CLM-3943-PK |
| L-LEUCINE (U-13C, 99%) | Cambridge Isotope Laboratories | Cat#CLM-2262-PK |
| Fatty acid free BSA | Sigma | Cat#A6003 |
| XBridge BEH Amide XP column | Waters | Cat#176002889 |
| Acquity UPLC BEH C18 column | Waters | Cat#186003719 |
| EDC | Sigma | Cat#03449 |
| 3-Nitrophenylhydrazine | Sigma | Cat#N21804 |
| Pyridine | Sigma | Cat#270970 |
| beta-mercaptoethanol | Sigma | Cat#M6250 |
| **Experimental Models: Organisms/Strains** | | |
| Mouse: C57BL/6 | Charles River Laboratories | Cat#027 |
| Pig: Yorkshire | Meck Swine LLC | N/A |
| **Software and Algorithms** | | |
| MAVEN software | http://genomics-pubs.princeton.edu/mzroll/index.php | Princeton University |

## Contact for Reagents and Resources Sharing

Further information and requests for resources and reagents should be directed to and will be fulfilled by the Lead Contact, Joshua Rabinowitz (joshr@princeton.edu).

## Experimental Model and Subject Details

**Pig experiments—**Pig studies followed protocols approved by the University of Pennsylvania Institutional Animal Care and Use Committee. Five-month old male Yorkshire pigs were fed at 4 PM and then overnight fasted. At 7 AM in the next morning, anesthesia was initiated with a ketamine IM injection (15~35 mg/kg), followed by intubation and maintenance of anesthesia with inhaled isoflurane at 0.5~5%. Infusion of [U-$^{13}$C]-glucose or [U-$^{13}$C]-lactate was performed via the external jugular vein catheter. Blood was collected from the carotid artery every 10 min during the infusion. For the glucose, after a bolus of 0.47 mL/kg of 200 mM solution, infusion was performed with 0.04 mL/min/kg of 26 mM solution for 110 min to achieve steady-state blood labeling (9%). For the lactate infusion,

infusion was performed with 0.035 mL/min/kg of 82 mM solution for 110 min to achieve steady-state blood labeling (11%). Arterial and venous access was obtained to enable fluid infusion (NaCl 4 - 10 mcg/kg/min), blood pressure monitoring, pharmacological control of blood pressure (0.2 - 2.0 mcg/kg/min dobutamine and 0.1 - 5.0 mcg/kg/min phenylephrine, as required), and blood sampling. The primary initiative venous access was via ultrasound-guided percutaneous puncture of the external jugular vein. Arterial access was through a neck to the carotid artery. The surgical site was blocked with Bupivacaine SQ just after the first incision. The subcutaneous tissues and muscle layers were carefully dissected, with hemostasis achieved with electrocautery. For blood sampling from the hepatic and the portal vein, a catheter was placed on each vein. Blood from inferior vena cava, internal jugular vein, femoral vein, renal vein, splenic vein, inferior pancreatic vein, inferior mesenteric vein, lateral auricular vein, and coronary sinus were obtained by drawing with a 27G needle connected to 1 mL syringe. Blood was drawn from each vessel twice at 1 - 2 min intervals, except for the coronary sinus (only a single draw). For urine, a catheter was implanted into the bladder, residual urine was drained, and a sterile 50 mL falcon tube was connected to the catheter to collect fresh urine. After completion of blood sampling, the animal was euthanized. Blood samples were placed at room temperature for 10 - 20 min, and centrifuged at 1,000 x g for 10 min to obtain serum.

**Mouse experiments—**Mouse studies followed protocols approved by the Princeton University Institutional Animal Care and Use Committee. Infusion was performed on single-housed 10 - 14 week old male C57BL/6 mice with a catheter surgically implanted on the right jugular vein (Charles River). $^{13}$C-citrate and $^{13}$C-acetate infusion solutions were prepared in saline with 20 mM [U-$^{13}$C]-sodium citrate, 5mM [U-$^{13}$C]-sodium malate, 10 mM [U-$^{13}$C]-sodium succinate, or 200 mM [U-$^{13}$C]-sodium acetate. Infusion was performed with 0.1 μL/g/min for 3 hours to achieve steady-state blood labeling (10~15%) without perturbation of circulating blood levels. For $^{13}$C-LCFA infusions, [U-$^{13}$C]-LCFA was first dissolved in 70°C saline at 16 mM and slowly mixed with 37°C saline containing 4 mM fatty acid-free BSA at 1:1 v/v ratio to conjugate LCFA to albumin at 4:1 ratio. Final infusion solutions were 8 mM for [U-$^{13}$C]-sodium oleate or [U-$^{13}$C]-sodium linoelate and 4 mM for [U-$^{13}$C]-sodium palmitate. Infusion was performed with 0.5 μL/g/min for 3 hours to achieve steady-state blood labeling (8~10%) without perturbation of circulating blood levels. The mouse infusion setup (Instech Laboratories, Plymouth Meeting, PA) included a tether and swivel system so that the animal has free movement in the cage. On the day of the experiment, mice were transferred to new cages without food at 10 AM for fasting. At 3 PM, infusion was started. Blood (~10 μL) was collected by tail bleeding in blood collection tubes (Sarstedt 16.443.100), placed on ice for 20 min, and centrifuged at 16,000 x g for 10 min at 4°C to obtain serum. For tissue harvest, mice were euthanized via cervical dislocation and tissues were quickly dissected and snap frozen in liquid nitrogen with a pre-cooled Wollenberger clamp. Serum and tissue samples were kept at -80°C until LC-MS analysis. All mouse experiments were performed with 2 or 3 mice per day, with results validated on multiple days using mice from different cages.

## Method Details

**Metabolite extraction—**Serum (5 μL) was mixed with 150 μL -20°C 40:40:20 methanol:acetonitrile:water (extraction solvent), vortexed, and immediately centrifuged at 16,000 x g for 10 min at 4°C. The supernatant was collected for LC-MS analysis. To extract metabolites from tissue samples, frozen tissue samples were ground at liquid nitrogen temperature with a Cryomill (Retsch, Newtown, PA). The resulting tissue powder (~20 mg) was weighed and then extracted by adding -20°C extraction solvent (as above), vortexed, and immediately centrifuged at 16,000 x g for 10 min at 4°C. The volume of the extraction solution (μL) was 40x the weight of tissue (mg) to make an extract of 25 mg tissue per mL solvent. The supernatant was collected for LC-MS analysis.

**Metabolite measurement by LC-MS—**A quadrupole-orbitrap mass spectrometer (Q Exactive, Thermo Fisher Scientific, San Jose, CA) operating in negative or positive ion mode was coupled to hydrophilic interaction chromatography via electrospray ionization and used to scan from m/z 70 to 1000 at 1 Hz and 75,000 resolution. LC separation was on a XBridge BEH Amide column (2.1 mm x 150 mm, 2.5 μm particle size, 130 Å pore size; Waters, Milford, MA) using a gradient of solvent A (20 mM ammonium acetate, 20 mM ammonium hydroxide in 95:5 water: acetonitrile, pH 9.45) and solvent B (acetonitrile). Flow rate was 150 μL/min. The LC gradient was: 0 min, 85% B; 2 min, 85% B; 3 min, 80% B; 5 min, 80% B; 6 min, 75% B; 7 min, 75% B; 8 min, 70% B; 9 min, 70% B; 10 min, 50% B; 12 min, 50% B; 13 min, 25% B; 16 min, 25% B; 18 min, 0% B; 23 min, 0% B; 24 min, 85% B; 30 min, 85% B. Autosampler temperature was 5°C, and injection volume was 3 μL. Data were analyzed using the MAVEN software. For tracer experiments, isotope labeling was corrected for natural $^{13}C$ abundance (Su et al., 2017).

**SCFA measurement—**SCFAs were derivatized and measured by LC-MS. The derivatizing reagent was 12 mM EDC, 15 mM 3-Nitrophenylhydrazine and pyridine (2% v/v) in methanol. Reaction was stopped with quenching reagent consisting of 0.5 mM beta-mercaptoethanol and 0.1% formic acid in water. Serum (5 μL) was mixed with derivatizing reagent (100 μL) and incubated for 1 hour at 4°C. Then, the samples were centrifuged at 16,000 x g for 10 min at 4°C, and 20 μL of supernatant was mixed with 200 μL of the quenching reagent. After centrifugation at 16,000 x g for 10 min at 4°C, supernatants were collected for LC-MS analysis. A quadrupole-time of flight mass spectrometer (Q-TOF, Agilent, Santa Clara, CA) operating in negative ion mode was coupled to C18 chromatography via electrospray ionization and used to scan from m/z 100 to 300 at 1 Hz and 15,000 resolution. LC separation was on an Acquity UPLC BEH C18 column (2.1 mm x 100 mm, 1.7 5 μm particle size, 130 Å pore size; Waters, Milford, MA) using a gradient of solvent A (0.01% formic acid in water) and solvent B (0.01% formic acid in isopropanol). Flow rate was 400 μL/min, except that from 6 min to 8 min flow rate was increased to 700 μL/min. The LC gradient was: 0 min, 10% B; 2 min, 15% B; 5 min, 25% B; 6 min, 100% B; 8 min, 100% B; 8.6 min, 10% B; 10.5 min, 10% B. Autosampler temperature was 5°C, and injection volume was 10 μL. Ion masses for derivatized formate, acetate, propionate, and butyrate were 180, 194, 208, and 222, respectively.

**Protein labeling measurement—**Infusion solution was prepared in saline with [U-$^{13}$C]-leucine, unlabeled valine and isoleucine (45, 37.5, and 26.25 mM, respectively), as previously described (Neinast et al., 2019). Infusion was performed for 2 hours at the rate of 0.0836 μL/g/min. Tissue proteins were isolated by chloroform-methanol extraction. Protein pellets were washed with methanol twice to remove residual amino acids. Then, the protein samples were hydrolyzed with 6 M HCl at 120°C overnight. After completely drying the HCl with blowing nitrogen gas, the samples were dissolved with 80% methanol in water, centrifuged at 16,000 x g for 10 min at 4°C, and supernatants were collected for LC-MS analysis.

### Quantification and Statistical Analysis

The absolute metabolite concentrations in the blood were taken from the Human Metabolome Database, using the average of healthy male data. Regional blood flow was from (PA, 2005). A two-tailed unpaired Student's t-test was used to calculate p-values. Metabolomics data were corrected for multiple comparisons, based on the number of measured metabolites, via the Benjamani-Hochberg method, with a false-discover rate (FDR) cut off of 0.05 used to determine statistical significance.

### Data and Software Availability

All the pig A/V data are provided in Data File 3. MAVEN software for LC-MS data analysis is available online at http://genomics-pubs.princeton.edu/mzroll/index.php.

## Supplementary Material

Refer to Web version on PubMed Central for supplementary material.

## Acknowledgements

C.J. is a postdoctoral fellow of the American Diabetes Association (1-17-PDF-076). S.H. is supported by a NIH grant K99DK117066. This work was supported by NIH Pioneer Award 1DP1DK113643 and Diabetes Research Center Grant P30 DK019525. We thank members of the Rabinowitz lab for scientific discussions.

## References

Ahn E, Kumar P, Mukha D, Tzur A, Shlomi T. Temporal fluxomics reveals oscillations in TCA cycle flux throughout the mammalian cell cycle. Mol Syst Biol. 2017; 13:953. [PubMed: 29109155]

Barrows BR, Timlin MT, Parks EJ. Spillover of dietary fatty acids and use of serum nonesterified fatty acids for the synthesis of VLDL-triacylglycerol under two different feeding regimens. Diabetes. 2005; 54:2668–2673. [PubMed: 16123356]

Baruch SB, Burich RL, Eun CK, King VF. Renal metabolism of citrate. Med Clin North Am. 1975; 59:569–582. [PubMed: 1092932]

Bascuñana P, Thackeray JT, Bankstahl M, Bengel FM, Bankstahl JP. Anesthesia and Preconditioning Induced Changes in Mouse Brain [18F] FDG Uptake and Kinetics. Mol Imaging Biol. 2019

Björntorp P. Adipose tissue distribution and function. Int J Obes. 1991; 15(Suppl 2):67–81.

Cantarow A, Ricchiuti G. Epinephrine Hyperglycemia. J Clin Invest. 1934; 13:461–478. [PubMed: 16694222]

Chambers ES, Preston T, Frost G, Morrison DJ. Role of Gut Microbiota-Generated Short-Chain Fatty Acids in Metabolic and Cardiovascular Health. Curr Nutr Rep. 2018; 7:198–206. [PubMed: 30264354]

Chantranupong L, Wolfson RL, Sabatini DM. Nutrient-Sensing Mechanisms across Evolution. Cell. 2015; 161:67–83. [PubMed: 25815986]

Chow WH, Devesa SS, Warren JL, Fraumeni JF. Rising incidence of renal cell cancer in the United States. JAMA. 1999; 281:1628–1631. [PubMed: 10235157]

Coggan AR. Use of stable isotopes to study carbohydrate and fat metabolism at the whole-body level. Proc Nutr Soc. 1999; 58:953–961. [PubMed: 10817163]

Cori CF. The glucose-lactic acid cycle and gluconeogenesis. Curr Top Cell Regul. 1981; 18:377–387. [PubMed: 7273846]

Davis MA, Williams PE, Cherrington AD. Effect of glucagon on hepatic lactate metabolism in the conscious dog. Am J Physiol. 1985; 248:E463–70. [PubMed: 2858980]

Ducker GS, Rabinowitz JD. One-Carbon Metabolism in Health and Disease. Cell Metab. 2017; 25:27–42. [PubMed: 27641100]

Eipel C, Abshagen K, Vollmar B. Regulation of hepatic blood flow: the hepatic arterial buffer response revisited. World J Gastroenterol. 2010; 16:6046–6057. [PubMed: 21182219]

Felig P, Wahren J. Amino acid metabolism in exercising man. J Clin Invest. 1971; 50:2703–2714. [PubMed: 5129318]

Felig P, Owen OE, Wahren J, Cahill GF. Amino acid metabolism during prolonged starvation. J Clin Invest. 1969; 48:584–594. [PubMed: 5773094]

Gentile CL, Weir TL. The gut microbiota at the intersection of diet and human health. Science (80-. ). 2018; 362:776–780.

Gottlieb E, Vousden KH. One carbon, many roads. Cell Death Differ. 2017; 24:193–194. [PubMed: 28060379]

Guo Z, Jensen MD. Intramuscular fatty acid metabolism evaluated with stable isotopic tracers. J Appl Physiol. 1998; 84:1674–1679. [PubMed: 9572816]

Hamm LL. Renal handling of citrate. Kidney Int. 1990; 38:728–735. [PubMed: 2232510]

Hickam JB, Cargill WH, Golden A. Cardiovascular Reactions to Emotional Stimuli. Effect on the Cardiac Output, Arteriovenous Oxygen Difference, Arterial Pressure, and Peripheral Resistance 1. J Clin Invest. 1948; 27:290–298. [PubMed: 16695554]

Hui S, Ghergurovich JM, Morscher RJ, Jang C, Teng X, Lu W, Esparza LA, Reya T, Le Zhan, Yanxiang Guo J, et al. Glucose feeds the TCA cycle via circulating lactate. Nature. 2017; 551:115–118. [PubMed: 29045397]

Ivanisevic J, Elias D, Deguchi H, Averell PM, Kurczy M, Johnson CH, Tautenhahn R, Zhu Z, Watrous J, Jain M, et al. Arteriovenous Blood Metabolomics: A Readout of Intra-Tissue Metabostasis. Sci Rep. 2015; 5

Jha P, McDevitt MT, Halilbasic E, Williams EG, Quiros PM, Gariani K, Sleiman MB, Gupta R, Ulbrich A, Jochem A, et al. Genetic Regulation of Plasma Lipid Species and Their Association with Metabolic Phenotypes. Cell Syst. 2018; 6:709–721.e6. [PubMed: 29909275]

Kikuchi T, Orita Y, Ando A, Mikami H, Fujii M, Okada A, Abe H. Liquid-chromatographic determination of guanidino compounds in plasma and erythrocyte of normal persons and uremic patients. Clin Chem. 1981; 27:1899–1902. [PubMed: 7296840]

Lundholm K, Bennegård K, Zachrisson H, Lundgren F, Edén E, Möller-Loswick AC. Transport kinetics of amino acids across the resting human leg. J Clin Invest. 1987; 80:763–771. [PubMed: 3624488]

Mithieux G. The new functions of the gut in the control of glucose homeostasis. Curr Opin Clin Nutr Metab Care. 2005; 8:445–449. [PubMed: 15930972]

Moore MC, Flakoll PJ, Hsieh PS, Pagliassotti MJ, Neal DW, Monohan MT, Venable C, Cherrington AD. Hepatic glucose disposition during concomitant portal glucose and amino acid infusions in the dog. Am J Physiol. 1998; 274:E893–902. [PubMed: 9612248]

Neinast MD, Jang C, Hui S, Murashige DS, Chu Q, Morscher RJ, Li X, Zhan L, White E, Anthony TG, et al. Quantitative Analysis of the Whole-Body Metabolic Fate of Branched-Chain Amino Acids. Cell Metab. 2019

Noronha A, Daníelsdóttir AD, Gawron P, Jóhannsson F, Jónsdóttir S, Jarlsson S, Gunnarsson JP, Brynjólfsson S, Schneider R, Thiele I, et al. ReconMap: an interactive visualization of human metabolism. Bioinformatics. 2017; 33:605–607. [PubMed: 27993782]

PA I. The Handbook of Cardiac Anatomy, Physiology and Devices. 2005

Perleberg C, Kind A, Schnieke A. Genetically engineered pigs as models for human disease. Dis Model Mech. 2018; 11

Poulianiti KP, Kaltsatou A, Mitrou GI, Jamurtas AZ, Koutedakis Y, Maridaki M, Stefanidis I, Sakkas GK, Karatzaferi C. Systemic Redox Imbalance in Chronic Kidney Disease: A Systematic Review. Oxid Med Cell Longev. 2016; 2016:1–19.

Prather RS, Shen M, Dai Y. Genetically modified pigs for medicine and agriculture. Biotechnol Genet Eng Rev. 2008; 25:245–265. [PubMed: 21412358]

Raimundo N, Baysal BE, Shadel GS. Revisiting the TCA cycle: signaling to tumor formation. Trends Mol Med. 2011; 17:641–649. [PubMed: 21764377]

Ricketts CJ, De Cubas AA, Fan H, Smith CC, Lang M, Reznik E, Bowlby R, Gibb EA, Akbani R, Beroukhim R, et al. The Cancer Genome Atlas Comprehensive Molecular Characterization of Renal Cell Carcinoma. Cell Rep. 2018; 23:3698.

Saltiel AR. Insulin Signaling in the Control of Glucose and Lipid Homeostasis. Handbook of Experimental Pharmacology. 2015:51–71.

Shlomi T, Cabili MN, Herrgård MJ, Palsson BØ, Ruppin E. Network-based prediction of human tissue-specific metabolism. Nat Biotechnol. 2008; 26:1003–1010. [PubMed: 18711341]

Simpson DP. Regulation of Renal Citrate Metabolism by Bicarbonate Ion and pH: Observations in Tissue Slices and Mitochondria*. J Clin Invest. 1967; 46:225–238. [PubMed: 6018760]

Sinturel F, Gerber A, Mauvoisin D, Wang J, Gatfield D, Stubblefield JJ, Green CB, Gachon F, Schibler U. Diurnal Oscillations in Liver Mass and Cell Size Accompany Ribosome Assembly Cycles. Cell. 2017; 169:651–663.e14. [PubMed: 28475894]

Smith RJ. Glutamine Metabolism and Its Physiologic Importance. J Parenter Enter Nutr. 1990; 14:40S–44S.

Stumvoll M, Meyer C, Perriello G, Kreider M, Welle S, Gerich J. Human kidney and liver gluconeogenesis: evidence for organ substrate selectivity. Am J Physiol. 1998; 274:E817–26. [PubMed: 9612239]

Su X, Lu W, Rabinowitz JD. Metabolite Spectral Accuracy on Orbitraps. Anal Chem. 2017

Sullivan LB, Martinez-Garcia E, Nguyen H, Mullen AR, Dufour E, Sudarshan S, Licht JD, Deberardinis RJ, Chandel NS. The Proto-oncometabolite Fumarate Binds Glutathione to Amplify ROS-Dependent Signaling. Mol Cell. 2013; 51:236–248. [PubMed: 23747014]

Teng L, Chen Y, Cao Y, Wang W, Xu Y, Wang Y, Lv J, Li C, Su Y. Overexpression of ATP citrate lyase in renal cell carcinoma tissues and its effect on the human renal carcinoma cells in vitro. Oncol Lett. 2018; 15:6967–6974. [PubMed: 29725424]

Thiele I, Swainston N, Fleming RMT, Hoppe A, Sahoo S, Aurich MK, Haraldsdottir H, Mo ML, Rolfsson O, Stobbe MD, et al. A community-driven global reconstruction of human metabolism. Nat Biotechnol. 2013; 31:419–425. [PubMed: 23455439]

Wahren J, Felig P, Cerasi E, Luft R. Splanchnic and peripheral glucose and amino acid metabolism in diabetes mellitus. J Clin Invest. 1972; 51:1870–1878. [PubMed: 5032528]

Wu GD, Compher C, Chen EZ, Smith SA, Shah RD, Bittinger K, Chehoud C, Albenberg LG, Nessel L, Gilroy E, et al. Comparative metabolomics in vegans and omnivores reveal constraints on diet-dependent gut microbiota metabolite production. Gut. 2016; 65:63–72. [PubMed: 25431456]

Europe PMC Funders Author Manuscripts

Europe PMC Funders Author Manuscripts

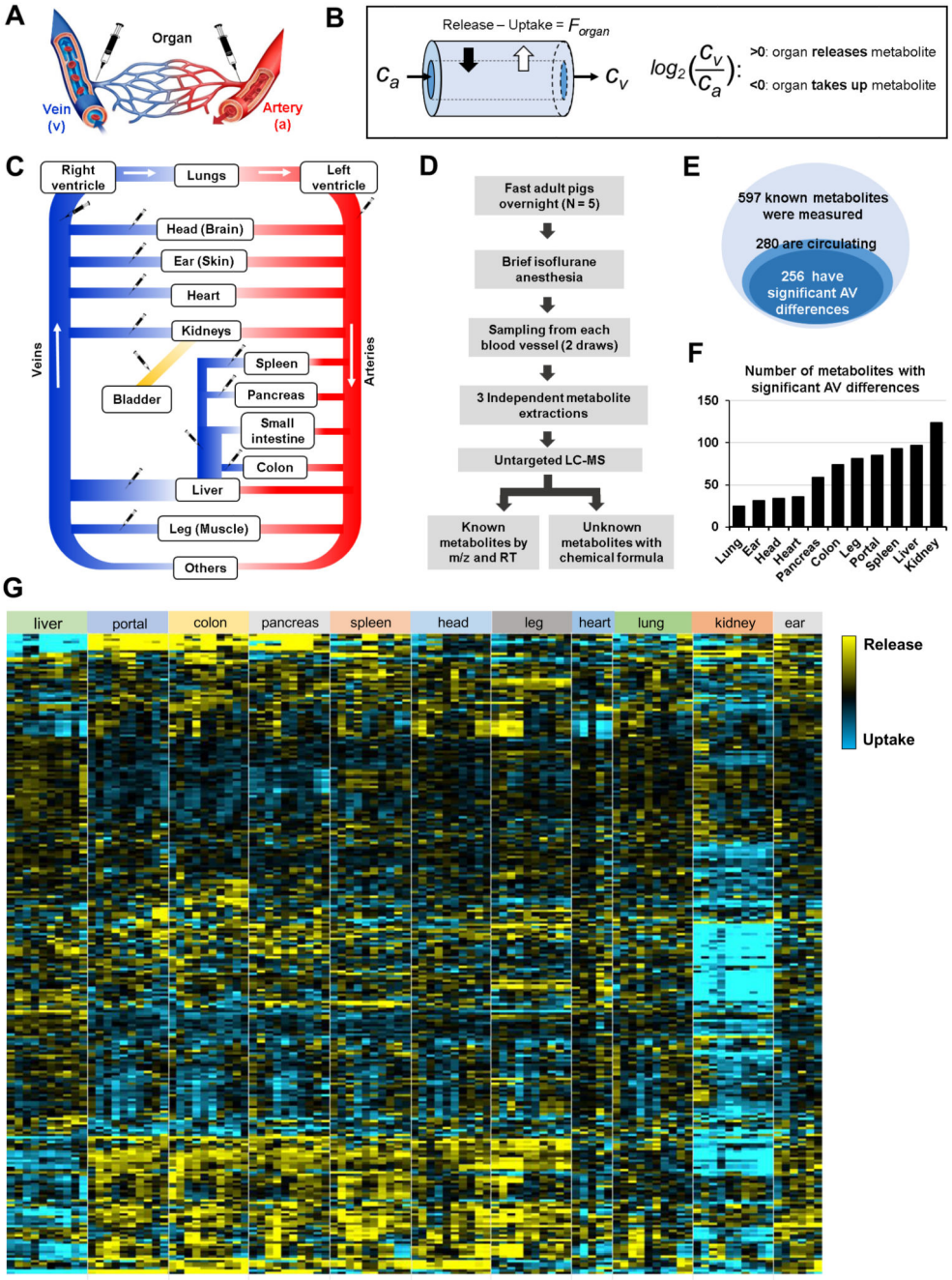


**Fig. 1. The landscape of metabolite exchange between organs.**

(**A**) AV difference measurements were achieved by sampling blood from the arterial circulation and organ-specific draining veins of fasting, anesthetized pigs. (**B**) The difference between metabolite production and consumption by an organ (the net flux, $F_{organ}$) results in enrichment or depletion of the metabolite in the exiting venous blood relative to entering arterial blood (concentrations $C_V$ and $C_a$). This concentration difference is measured by LC-MS and reported as a log fold change. (**C**) Schematic of the circulatory system. Syringes indicate blood sampling sites. (**D**) Workflow. (**E**) Venn diagrams of measured metabolites,

circulating metabolites, and metabolites with significant AV differences. (**F**) Number of metabolites with significant AV differences for each organ. (**G**) Heat map of AV differences of circulating metabolites across organs. Yellow indicates release and blue indicates uptake. Each data point indicates median of three technical replicates, with independent duplicate blood draws from the same pig shown separately (N = 5 pigs and 10 data points for most organs; only a single blood draw per pig was performed in the heart and only 3 pigs were used for the ear vein sampling). Leg, head, and ear primarily reflect skeletal muscle, brain, and skin metabolism, respectively. See also Figures S1, S2, and Data Files 1-3.



Europe PMC Funders Author Manuscripts

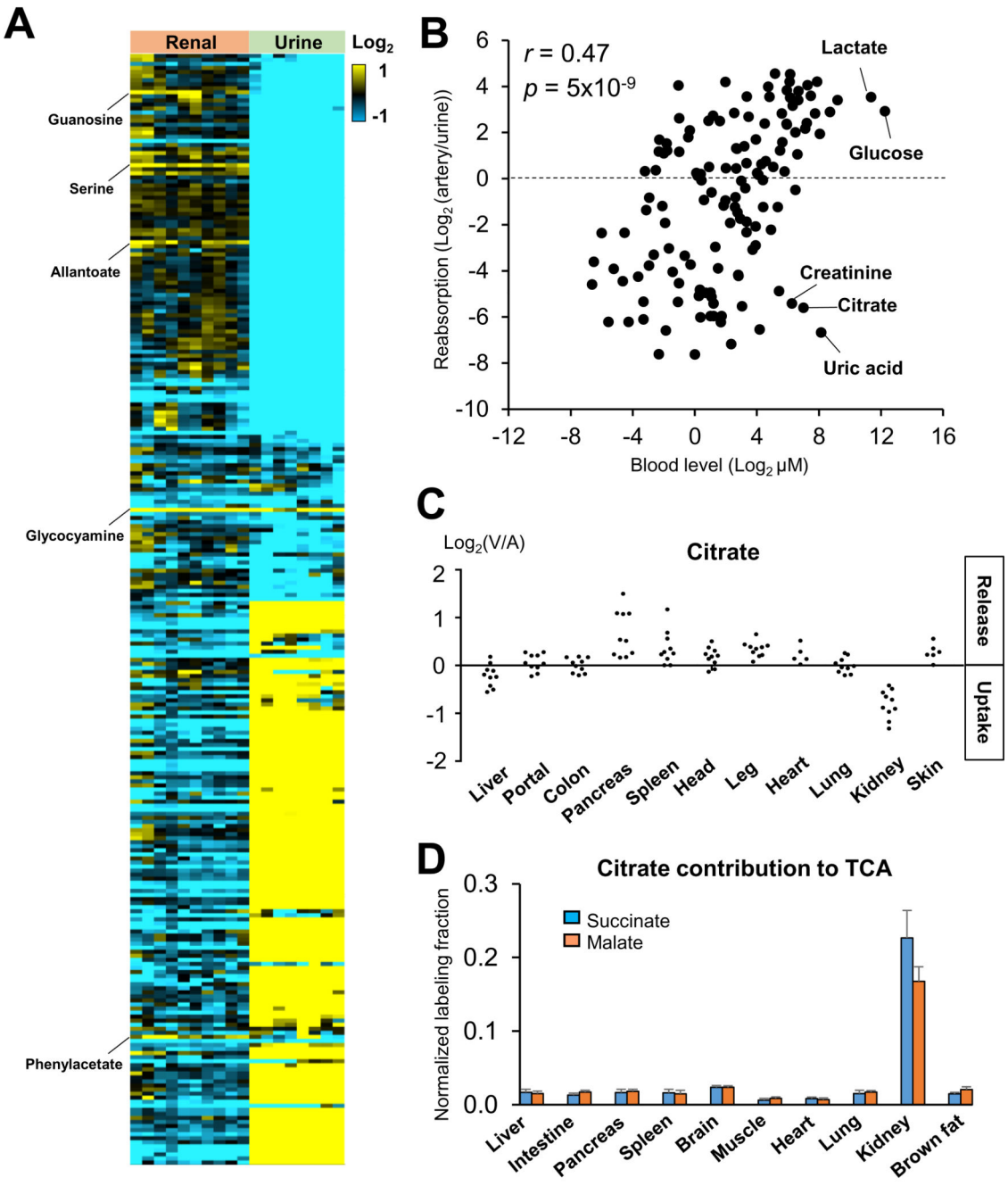


**Fig. 2. The kidneys clear most metabolites, with citrate a kidney-specific fuel.**

(**A**) Heat map of metabolite abundance ($log_2$) in renal vein relative to the arterial blood (left) or urine relative to arterial blood (right) in pigs. Metabolites produced by the kidneys are highlighted on the left. (**B**) Correlation between a metabolite's blood concentration and reabsorption efficiency. (**C**) AV difference of citrate across the indicated organs in pigs. Each data point reflects an independent venous blood draw. (**D**) Citrate contribution to TCA in mice. The kidneys are unique in using citrate as fuel. Mice were intravenously infused with [U-$^{13}$C]-citrate, and average TCA intermediate carbon labeling was normalized to blood

citrate labeling. Data are means and error bars are standard errors (N = 4 mice). See also Figure S3.



Europe PMC Funders Author Manuscripts

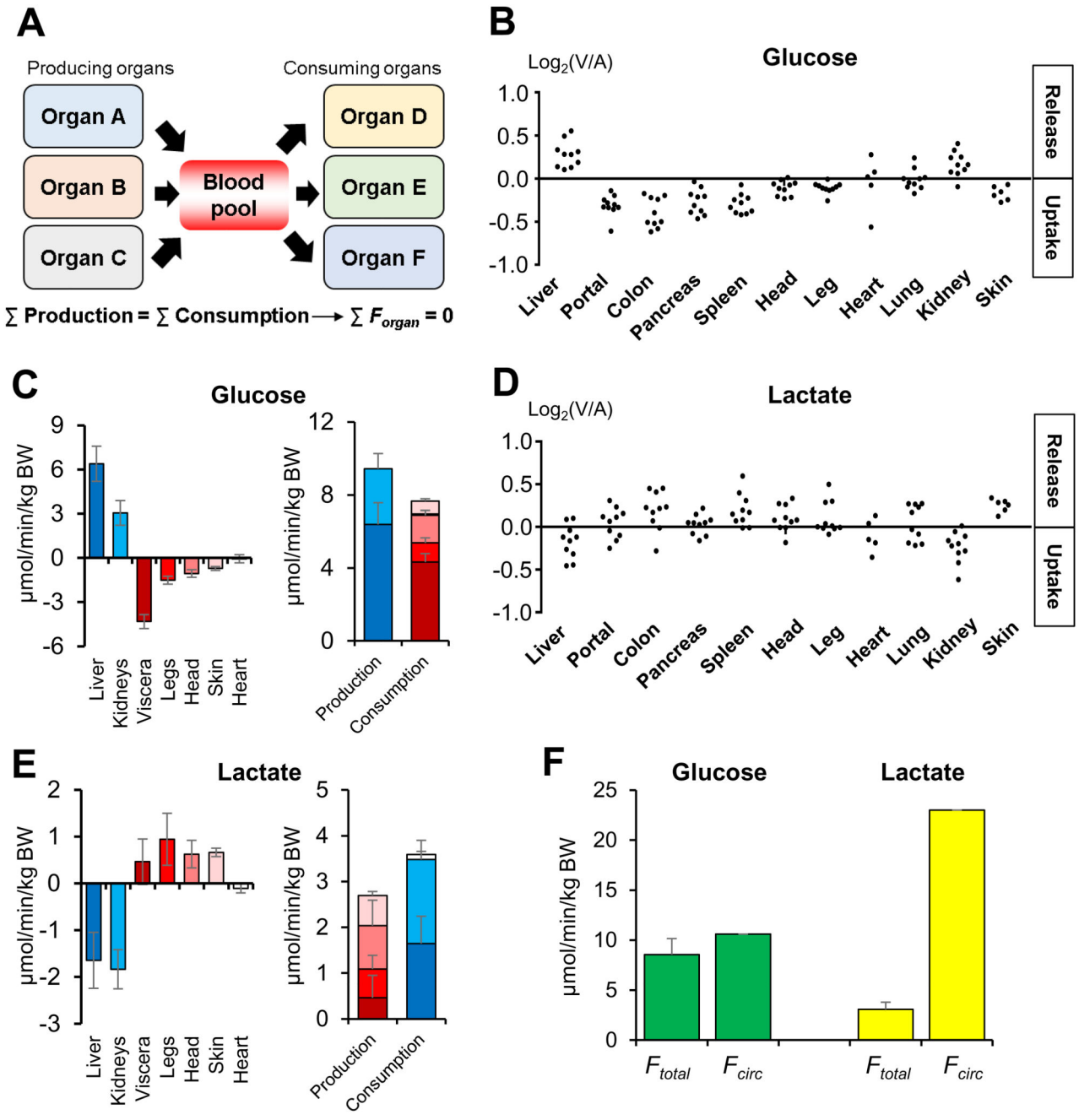


**Fig. 3. Glucose production localizes to the liver and kidneys, whereas lactate production is distributed throughout the body.**

(**A**) Metabolite production and consumption across all organs must balance to maintain circulating metabolite homeostasis. (**B, D**) Glucose and lactate show the opposite exchange patterns. Each data point reflects an independent venous blood draw from pig. (**C, E**) Production and consumption fluxes of glucose and lactate in pigs. (**F**) Comparison between sum of organ production fluxes ($F_{total}$) and whole body production rate ($F_{circ}$) of glucose and lactate in pigs. Note that $F_{total}$ and $F_{circ}$ are similar for glucose but different for lactate,




Europe PMC Funders Author Manuscripts

indicating simultaneous lactate production and consumption within the same organ. Data are means and error bars are standard errors (N = 5 pigs, except for isotope tracing, which was performed in a single pig). BW, body weight; Viscera, organs feeding into the hepatic portal vein. See also Figure S4.



Europe PMC Funders Author Manuscripts

Europe PMC Funders Author Manuscripts

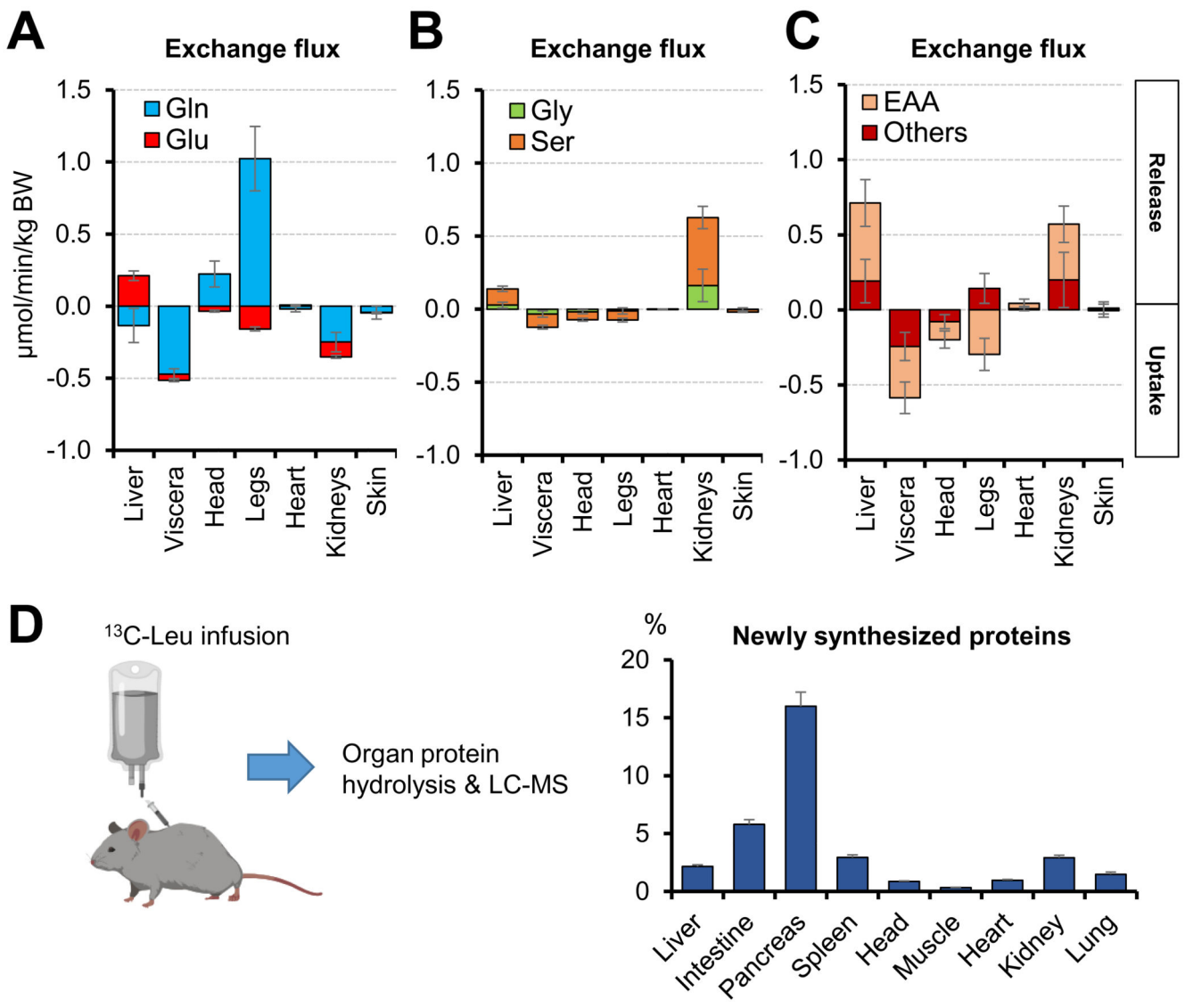


**Fig. 4. The liver and kidneys release amino acids, which are consumed substantially by the other visceral organs.**

(**A-C**) Exchange fluxes of the indicated amino acids in pigs. Data are means and error bars are standard errors (N = 5 pigs). "Others" refers to Ala, Pro, Arg and Tyr. (**D**) Newly synthesized proteins in mice. Visceral organs (intestine, pancreas, and spleen) show the most active protein synthesis. Mice were intravenously infused with [U-$^{13}$C]-leucine for 2 h and protein leucine labeling was normalized to blood leucine labeling. Data are means and error bars are standard errors (N = 8 mice). See also Figure S5.

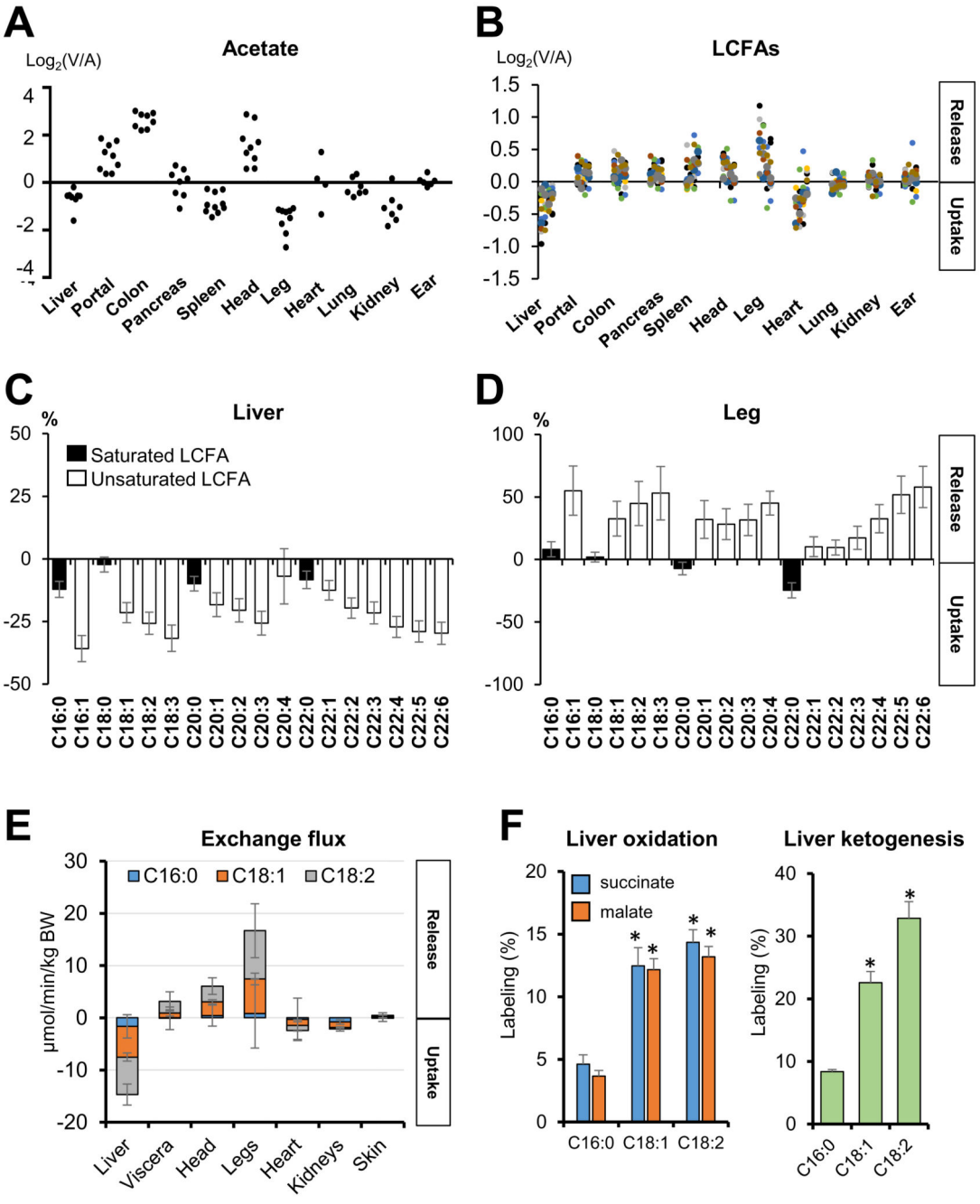


**Fig. 5. The liver preferentially consumes and burns unsaturated as opposed to saturated fatty acids.**

(**A**) Acetate is released from the gut and head. Each data point reflects an independent venous blood draw from pig. (**B**) LCFAs are released from the visceral organs other than liver, head, and leg, and consumed by the liver and heart. Each data point reflects the mean AV difference for a specific LCFA in pigs, with different fatty acids shown by different colors. (**C, D**) The liver and leg show the opposite preferences in LCFA uptake. (**E**) Exchange fluxes of the three most abundant LCFAs in pigs. (**F**) The liver preferentially

oxidizes unsaturated LCFAs in mice. Mice were intravenously infused with the indicated [U-$^{13}$C]-LCFA, and fractions of total labeled carbons in TCA intermediates and 3-hydroxybutyate in the liver were normalized to blood tracer labeling. Data are means and error bars are standard errors. For panels **A-E**, N = 5 pigs. For panel **F**, N = 4, 6, and 7 mice for C16:0, C18:1, and C18:2 infusions, respectively. *$p$<0.01 by two-tailed Student's $t$-test. Viscera, organs feeding into the hepatic portal vein. See also Figure S6.



Europe PMC Funders Author Manuscripts

## Table 1

**Selected examples of organ-specific metabolite production and consumption.**

See also Data File 1.

| Organ | Production | | Consumption | |
|---|---|---|---|---|
| | **Metabolite** | **$Log_2$ (V/A)** | **Metabolite** | **$Log_2$ (V/A)** |
| Liver | Glutamate | 0.64 ± 0.11 | Bile acids (5) | -2.89 ± 0.19 |
| | Triethanolamine | 0.49 ± 0.17 | Phenylpropionic acid (2) | -2.29 ± 0.12 |
| | Acetoacetate | 0.38 ± 0.09 | Short-chain fatty acids (3) | -2.02 ± 0.83 |
| Portal (Intestine) | Bile acids (6) | 3.28 ± 0.21 | 2-Methylhippuric acid | -0.69 ± 0.15 |
| | Phenylpropionic acid (2) | 2.84 ± 0.32 | Glucose | -0.31 ± 0.05 |
| | Short-chain fatty acids (3) | 2.82 ± 1.15 | Glutamine | -0.28 ± 0.02 |
| Colon | Short-chain fatty acids (3) | 4.65 ± 1.21 | 2-Methylhippuric acid | -0.60 ± 0.21 |
| | Lithocholic acid | 4.04 ± 1.10 | 5-Hydroxylysine | -0.41 ± 0.05 |
| | Phenylpropionic acid (2) | 3.42 ± 0.48 | Glucose | -0.39 ± 0.05 |
| Pancreas | Xanthine | 1.05 ± 0.26 | 5-Hydroxylysine | -0.79 ± 0.19 |
| | Capryloyl glycine | 0.51 ± 0.09 | N-Carbamoylsarcosine | -0.39 ± 0.09 |
| | TCA intermediates (5) | 0.36 ± 0.17 | Amino acids (8) | -0.36 ± 0.01 |
| Spleen | O-Phosphorylethanolamine | 1.11 ± 0.22 | Adenosine | -0.61 ± 0.14 |
| | Nucleosides (9) | 0.52 ± 0.03 | Dihydroxymandelic acid | -0.33 ± 0.07 |
| | C22, C24 very long-chain fatty acids (11) | 0.35 ± 0.008 | C5 Acylcarnitine | -0.26 ± 0.02 |
| Head (brain) | Synephrine | 1.89 ± 0.68 | Dihydroxymandelic acid | -0.38 ± 0.12 |
| | Gluconolactone, Gluconate | 1.66 ± 0.03 | 2-Methylhippuric acid | -0.34 ± 0.11 |
| | Acetate | 1.46 ± 0.39 | Glutamate | -0.30 ± 0.09 |
| Leg (muscle) | Hypotaurine | 0.69 ± 0.12 | Glutamate | -1.41 ± 0.33 |
| | Branched chain hydroxyl acids (2) | 0.65 ± 0.12 | Ketone bodies (2) | -0.58 ± 0.14 |
| | Medium and long-chain | 0.57 ± 0.02 | Short-chain | -0.36 ± 0.05 |
| | acylcarnitines (11) | | acylcarnitines (5) | |
| Lung | 2-Phenylpropionic acid | 0.48 ± 0.14 | 5-Keto-D-gluconic acid | -0.31 ± 0.07 |
| | Aconitate | 0.26 ± 0.03 | Kynurenate | -0.22 ± 0.03 |
| | C22:0, C24:0 fatty acids | 0.24 ± 0.02 | 3-Hydroxyanthranilic acid | -0.17 ± 0.02 |
| Kidney | Glycocyamine | 1.87 ± 0.12 | N-Formyl-L-methionine | -2.66 ± 0.32 |
| | Serine | 0.73 ± 0.12 | Medium-chain | -2.61 ± 0.19 |
| | | | acylcarnitines (4) | |
| | Allantoate | 0.53± 0.12 | N-acetyl amino acids (9) | -1.27 ± 0.87 |
| Heart | Hypotaurine | 0.34 ± 0.11 | 3-Phenylpropionic acid | -0.71 ± 0.24 |
| | Glutamate | 0.26 ± 0.04 | Unsaturated long-chain fatty acids (11) | -0.53 ± 0.06 |
| | Biotin | 0.25 ± 0.06 | Hydroxyindoleacetic acid | -0.47 ± 0.12 |
| Ear (skin) | Guanine | 0.82 ± 0.19 | Hydroxyhippuric acid | -0.35 ± 0.08 |
| | Taurine | 0.53 ± 0.08 | Indole metabolites (2) | -0.23 ± 0.02 |
| | Long-chain | 0.20 ± 0.04 | Serine | -0.15 ± 0.01 |

| Organ | Production | | Consumption | |
|---|---|---|---|---|
| | **Metabolite** | **$Log_2$ (V/A)** | **Metabolite** | **$Log_2$ (V/A)** |
| | acylcarnitines (3) | | | |



Europe PMC Funders Author Manuscripts

## Table 2

**Top three metabolites produced and consumed by each organ in pigs.**

Ranking is based on multiplying the log2 (t-value) and log2 (V/A) to reflect both statistical significance and fold change. Numbers in parentheses refer to the number of metabolites in that category showing statistically significant AV differences across the indicated organ. All AV differences included in the table are statistically significant (FDR < 0.05).

| Organ | Exemplary discovery | Key evidence |
|---|---|---|
| Liver | Clears unsaturated fatty acids | Compared to the most abundant saturated fatty acids, oleate (C18:1) and linoleate (C18:2) show greater uptake and TCA contribution |
| | Produces amino acids | Significant release of amino acids |
| Intestine | Consumes glucose and amino acids | Greatest absolute uptake flux, of any organ, of both glucose and amino acids |
| Pancreas | Produces TCA intermediates | Significant release of citrate, ketoglutarate, succinate, fumarate, and malate |
| Spleen | Produces nucleosides | Significant release of cytidine, deoxycytidine, deoxyuridine, guanosine, inosine, thymidine, uridine, xanthosine |
| | Produces unsaturated very long chain fatty acids | Significant release of C22:1, C22:2, C22:3, C22:4, C22:5, C22:6, C24:1, C24:2, C24:3, C24:4, C24:5 |
| Brain | Produces acetate | > 2x increase in acetate in jugular vein blood |
| Leg muscle | Consumes short chain acylcarnitines | Significant uptake of C2:0, C3:0, C4:0, C5:0, C5:1 carnitines |
| | Produces long chain acylcarnitines | Significant release of C8:0, C10:0, C12:0, C12:1, C14:1, C14:2, C16:0, C16:1, C18:1, C18:2, C20:4 carnitines |
| Heart | Consumes long chain fatty acids | Significant uptake of C16:0, C16:1, C18:0, C18:1, C18:2, C20:1, C20:2, C22:4, C24:0, C24:1 |
| Lung | Produces saturated very long chain fatty acids | Significant release of C22:0, C24:0 |
| Kidney | Consumes citrate | Only organ with significant citrate uptake; TCA contribution from citrate > 10x higher than any other organ |
| | Maintains circulating pyruvate/lactate ratio | Significant increase in pyruvate relative to lactate in renal vein blood |
| | Produces amino acids | Significant release of amino acids |
| | Consumes medium and long chain acylcarnitines | Significant uptake of C5:0, C6:0, C8:0, C10:0, C10:1, C12:0, C12:1, C14:0, C14:1, C14:2, C16:1 (without release into urine) |